Journal of Solar Energy Research (JSER)

Journal homepage: www.jser.ut.ac.ir

A Local control scheme for voltage harmonic compensation and improvement of reactive and harmonic powers sharing for PV inverters with LCL filter in islanded microgrids

Reza Ghanizadeh

Department of Electrical Engineering, Urmia Branch, Islamic Azad University, Urmia, Iran

ARTICLE INFO

Article Type:

Research Artical

Received:26.12.2024
Accepted:19.01.2025

Keywords:
Photovoltaic;
Microgrid;
Droop controller;
Virtual impedance;
Load sharing;
Voltage quality

A B S T R A C T

This paper proposes a local control scheme to improve voltage quality and achieve accurate reactive and harmonic power sharing for photovoltaic (PV) inverters with *LCL* filters in an islanded microgrid (MG). The proposed control structure uses a modified reactive power-voltage (*Q-E*) droop controller to achieve reactive power sharing and prevent overloading of PV inverters, where the droop coefficient is precisely adjusted by considering the limited inverter capacity and the harmonic power of the load. Additionally, an adaptive virtual impedance (VI) loop is employed in the structure to compensate voltage harmonics and improve the sharing of fundamental and harmonic current components among the PV inverters. The proposed adaptive VI loop, based on the circulating currents of the fundamental and harmonic components, adaptively enhances the sharing of reactive and harmonic powers. In contrast to conventional VI schemes, where load sharing is achieved at the cost of additional harmonic voltage distortions, the proposed adaptive VI structure has a minimal impact on the output voltage quality of the PV inverters. The design process and parameter determination of the proposed structure are thoroughly explained, and simulation results in MATLAB/Simulink are provided to demonstrate the effectiveness of the proposed method.

1. Introduction

The integration of distributed generation (DG) sources, including photovoltaic (PV) systems, wind turbines, and energy storage systems, as an innovative solution plays a significant role in reducing dependency on fossil fuels, minimizing emissions, decreasing losses, and enhancing the stability of power distribution systems [1]. To overcome the technical challenges associated with

*Corresponding Author Email: reza.ghanizadeh@iau.ac.ir

Cite this article: Ghanizadeh, R. (2024). A Local control scheme for voltage harmonic compensation and improvement of reactive and harmonic powers sharing for PV inverters with LCL filter in islanded microgrids. Journal of Solar Energy Research, 9(4), 2062-2079. doi: 10.22059/jser.2025.387597.1510

DOI: 10.22059/jser.2025.387597.1510

integrating these sources into distribution systems, the concept of microgrids (MGs) has been introduced [2]. MGs can operate either in island mode or while connected to the main grid [3]. The importance of MGs lies in their ability to provide high flexibility in energy supply, demand management, and reduce stress on main grids.

In MGs, to ensure a stable and robust connection of PVs, an *LCL* filter is typically employed after the PV interfacing inverter. However, with nonlinear loads, the current flowing through the output inductor (L_o) can cause distortion in the output voltage of the *LCL* filter [4]. These distortions can damage sensitive equipment; therefore, compensating for harmonic voltage and current distortions in these networks is critically important**.** Moreover, when multiple PV interfacing inverters are used for harmonic compensation, the compensation efforts and load power must be appropriately distributed among these inverters. This approach enhances the efficiency, stability, and reliability of the system, ensuring that the MG performs effectively under various conditions, including nonlinear and unbalanced loads.

Various strategies have been proposed in previous works to improve voltage quality in MGs and enhance the sharing of fundamental and harmonic components of load power among DGs. Moussa et al. [5] proposed a harmonic compensation and load current sharing strategy for DGs. By adjusting the harmonic voltage reference based on harmonic power, inverters can autonomously distribute the harmonic current, eliminating the need for communication links. However, due to the open-loop operation of the controller, the inverter only absorbs a fraction of the harmonic current. Sreekumar et al. [6] have proposed an improved method for harmonic current sharing. The advantage of this method is that its performance is not influenced by the inner loop controller. However, the method is highly sensitive to variations in system parameters**.** Lorzadeh et al. [7]s have proposed a closed-loop harmonic current sharing scheme utilizing a secondary control layer. The primary advantage of this scheme lies in its high accuracy in current sharing, achieved through a closed-loop control mechanism. Mahmoud et al. [8] have proposed a control strategy aimed at improving the accuracy of reactive power sharing in islanded MGs. This strategy involves incorporating a communication link into the concept of VI. In this approach, the communication link is utilized to adjust the VIs for addressing the voltage drop mismatches among feeders, instead of directly matching the physical impedances of the feeders. In [9], the output voltage of each DG unit is adjusted by adding two terms: the reactive power sharing error reduction term and the voltage recovery term. The voltage recovery term is applied to compensate for the voltage drop caused by the reactive power sharing error reduction term. In [10], a high-frequency harmonic voltage signal is introduced into the output voltage reference of each DG unit to minimize reactive power sharing errors and enhance the accuracy of harmonic current distribution. This approach ensures precise power sharing by fine-tuning the closed-loop output impedance of each inverter, governed by the bandwidth of the voltage control loop. Pham et al. [11] have proposed a VI scheme to compensate for line impedance mismatches and enhance MG stability. In this scheme, both virtual resistance and inductance are simultaneously adjusted, improving system damping through precise power sharing. An enhanced voltage-intensity controller (VIC) have been proposed by Hang et al. [12] to achieve precise harmonic power sharing and harmonic voltage compensation in an islanded MG. This improved VIC employs straightforward integral controllers with two adjustable components, eliminating the need for feeder impedance or load current information. Wang et al. [13] have proposed a control strategy for the allocation of harmonic and unbalanced power among DGs in an MG, aiming to optimize power quality by adjusting the output impedance of DGs. The proposed strategy involves simultaneous tuning of the real and imaginary components of the VI and employs a closed-loop structure to ensure secure adjustments. Vijay et al. [14] have proposed a decentralized adaptive technique for adjusting the VI in a DG controller based on its output current, without requiring communication links, additional sensors, or estimation of network/load parameters. Wang et al. [15] have introduced a distributed secondary control scheme to ensure accurate reactive power sharing in multi-bus islanded MGs. This approach utilizes consensus control to dynamically adjust the virtual output impedance (VOI) for reactive power correction. The adaptive control structure based on VOI is inherently nonlinear. Liang et al. [16] have proposed a virtual synchronous generator (VSG) control approach based on adaptive VI for grid-connected and islanded MGs to mitigate inverter output impedance mismatches and improve proportional reactive power sharing among DGs. The VI consists of an adaptive virtual resistance and a fixed virtual inductance, where the virtual

resistance is adaptively designed based on the MG's operating points. Xiao et al. [17] have proposed a distributed philosophy-based VI modulation strategy for AC MGs with resistive feeders. The proposed method adjusts the fundamental and harmonic impedance to the desired values by exchanging information with neighboring inverters. Deng et al. [18] have proposed a decentralized current-sharing strategy leveraging iterative VI regulation (IVIR). The IVIR process is executed through multiple continuous iterations, each comprising three distinct stages. In the first stage, a VI increment is calculated based on the integral of the uniform output currents of the inverters. The second stage introduces impedance compensation to restore the voltage magnitude. In the final stage, the current-sharing error is assessed. This iterative adjustment effectively eliminates impedance mismatches with minimal VIs, ensuring accurate distribution of balanced, unbalanced, and harmonic currents while preserving high voltage quality. An et al. [19] have proposed a successive approximation-based VI regulation method for accurately compensating line impedance mismatches. Initially, each DG unit generates an adaptive VI adjustment derived from the error between the actual reactive power output and its reference, integrated with the conventional *Q-E* droop control. These two control mechanisms then operate alternately over multiple cycles. During each cycle, the reactive power reference for VI adjustment is updated based on the latest estimation from the *Q-E* droop control. This sequential process optimizes the VI of each DG unit, enabling precise power sharing among the units using only local information. Wang et al [20] have proposed an adaptive harmonic VI (HVI) control to enhance the voltage quality of MGs. The main goal of this study is to maximize harmonic power absorption by optimizing the minimum output impedances of inverters. To accomplish this, the proposed control strategy dynamically adjusts the harmonic voltage injection (HVI) of each inverter according to its operating conditions. Furthermore, a Monte Carlo-based harmonic power flow evaluation is implemented to analyze the practical effectiveness of the proposed control approach. Chen et al. [21] have proposed a complex VI method based on a P-$\dot{V}$ droop controller to decouple power components and enhance power-sharing accuracy among DG units. Nandi et al. [22] have introduced a dual and independent control system for interface converters, which automatically adjusts to either voltage control or current control mode, making it suitable for both islanded and grid-connected operations. In this scheme, an advanced angle control based on adaptive VI is proposed for voltage-controlled inverters, considering the interaction between active and reactive power and power disturbances on the source side. This controller minimizes power-sharing errors and enhances the rapid power adjustment process among DG units under various dynamic power conditions. Zhang et al. [23] have proposed a nonlinear droop scheme between harmonic remaining capacity (HRC) and VI to enhance the accuracy of harmonic power sharing and optimize the utilization of DG capacity. In this scheme, the HRC is defined and utilized for harmonic power sharing. Various operating conditions of the main load and the corresponding control objectives are analyzed to determine the variable droop coefficient. Consequently, this scheme optimizes the converter capacity utilization and dynamically and adaptively manage the inherent conflicts. Ndeh et al. [24] have proposed a nonlinear control strategy based on NARX neural network droop control (NARX-NN DBC) to improve reactive power sharing. This strategy is independent of varying line impedances and droop coefficients for different DGs and is less influenced by variable loads in the network. Mishra et al. [25] have introduced an innovative decentralized droop-based control scheme to address power-sharing challenges in an islanded AC MG powered by PV panels. This novel approach combines an enhanced VI control loop with traditional P-F/Q-V control loops. AlSadat et al. [26] have proposed an innovative method for accurate reactive power sharing by leveraging low-bandwidth communication through power lines. This approach utilizes communication signals to automatically adjust the VIs of inverters, ensuring precise reactive power distribution. Li et al. [27] have proposed an adaptive VI regulation (AVIR) strategy to improve reactive and harmonic power sharing. Goh et al [28] have presented a method for generating harmonic VI to address line impedance mismatches and limitations caused by various nonlinear loads. This method reduces the harmonic voltage at the point of common coupling (PCC) while simultaneously enabling harmonic current sharing. Kim et al [29] have proposed an adaptive regulation method for harmonic VI to achieve accurate harmonic power sharing. This method utilizes a consensus algorithm to dynamically adjust the harmonic VI based on the harmonic power sharing error among DGs, while accounting for line impedance mismatches. Notably, it operates without requiring prior knowledge of the line impedances. Hagshenas [30] has proposed a novel control

strategy to ensure power quality in PV-based islanded MGs. In this strategy, each PV system operates with two control levels: primary and secondary. The primary control level includes fundamental and harmonic VI loops, which enhance the sharing of fundamental power and distortion power among PV inverters, respectively. Hosseinpour et al. [31] have proposed a method for improving the power quality of photovoltaic arrays by focusing on the use of current sensors and VI shaping. In this approach, the output impedance of the system is divided into active and passive components. The active component is neutralized by applying series VIs, while its adverse effects are mitigated through parallel VIs.

In general, previous studies have proposed several significant control methods for compensating voltage and current harmonics and improving power sharing in MGs. However, fewer studies have focused on MGs employing inverters with *LCL* filters. In earlier works, VI schemes have been utilized to improve the sharing of fundamental and harmonic powers. The main challenge with these schemes is that achieving proper power sharing comes at the cost of voltage drops and additional harmonic distortions at the outputs of the DGs. Another aspect that has not been thoroughly studied in previous works is the effectiveness of these methods in reducing circulating fundamental and harmonic currents among the inverters of DGs. It is important to note that controlling circulating currents is essential to maintain the stability of an islanded MG and to enhance the quality of power sharing, thereby preventing the overloading of DG inverters.

In this paper, a method for modifying the *Q-E* droop controller is proposed to achieve ideal reactive power sharing and prevent the overloading of PV inverters in islanded MGs with arbitrary structures. In this approach, the droop coefficients are adjusted considering the limited capacity of inverters and harmonic power conditions. Furthermore, to compensate for voltage harmonics at the output of PVs, enhance the accuracy of sharing fundamental and harmonic current components of the load, and reduce circulating currents among PVs, an adaptive VI scheme is proposed for PVs equipped with LCL filters. The advantage of this scheme compared to conventional VI approaches lies in the fact that the output voltage quality of PVs is not significantly affected by proposed VI loops. This is because the proposed VI loops are placed in the feedback path of circulating harmonic and fundamental currents rather than in the path of the total load currents. Moreover, the proposed VI can improve the sharing of these load current components without requiring knowledge of the MG topology, such as the impedances of PV distribution lines. The main contributions of this paper are as follows:

- Proposing a modified *Q-E* droop control scheme to enhance reactive power sharing and prevent the overloading of PV inverters.
- Designing a VI scheme to compensate for harmonic voltage and improve the distribution of fundamental and harmonic components of load current among PVs.

2. Local Control Structure of PV Inverters with *LCL* Filter in an islanded MG

Figure 1 illustrates the general schematic of an islanded MG. As shown, each PV unit is equipped with a local controller, which communicates with others through a low-bandwidth communication (LBC) link. The use of LBC aims to avoid reliance on high-bandwidth communication, which could compromise the reliability of the control system. Moreover, LBC can be implemented at a relatively low cost. To ensure the adequacy of low bandwidth, the transmitted data must primarily consist of quasi-dc signals [32]. Therefore, the output current components of the PV units should be extracted in the *dq* reference frame and transmitted via the LBC to the local control levels of the PV units.

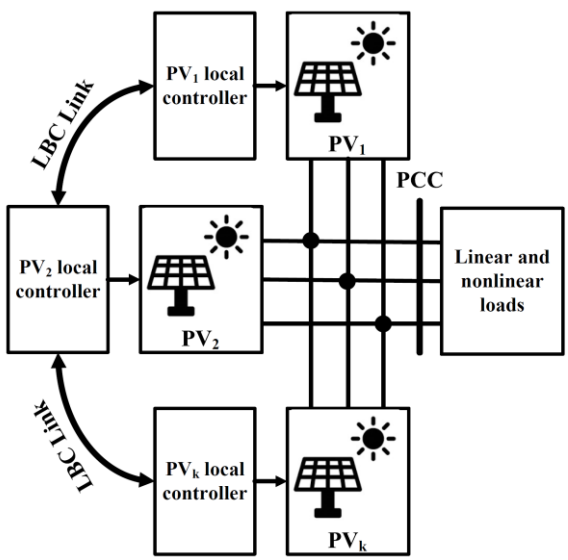

Figure 1. A general schematic of an islanded MG based on PV units

The details of the power stage and control structure of PV inverters in an islanded MG are

shown in figure 2. As observed, the power stage of each PV system includes a three-phase PWM inverter and an *LCL* filter. The control system operates in a stationary ($\alpha\beta$) reference frame, utilizing Clarke's transformation equations to convert voltages and currents between the abc and $\alpha\beta$ reference frames. Additionally, the MG consists of balanced linear and nonlinear loads, collectively considered at the PCC. Under these conditions, the output current and voltage of PV inverters contain odd harmonics (*5th*, *7th*, etc.). The local control structure of the PV inverters includes proportional-resonant (PR) controllers for voltage and current, modified droop controllers for active and reactive power, and an adaptive VI scheme. The control structure and equations of PR controllers are comprehensively detailed in reference [33].

The block structure of the measurement system is illustrated in figure 2. As shown, the fundamental and harmonic components of the output current from PV inverters are selectively extracted in the *dq* reference frame and transmitted to the local controllers of all PV units via an LBC link. In the simulation, a *1ms* delay in data transmission through the LBC link is assumed. Notably, voltage harmonic compensation is selectively applied to the dominant harmonics (*5th* and *7th*) of the current. Savaghebi et al. [34] have investigated the effect of low-bandwidth communication (LBC) link delay on the performance of the control system in improving voltage quality for various delays (1, 4, 7, and 10 ms). The results have demonstrated that as the delay increases, only a very small error is introduced when tracking the reference values.

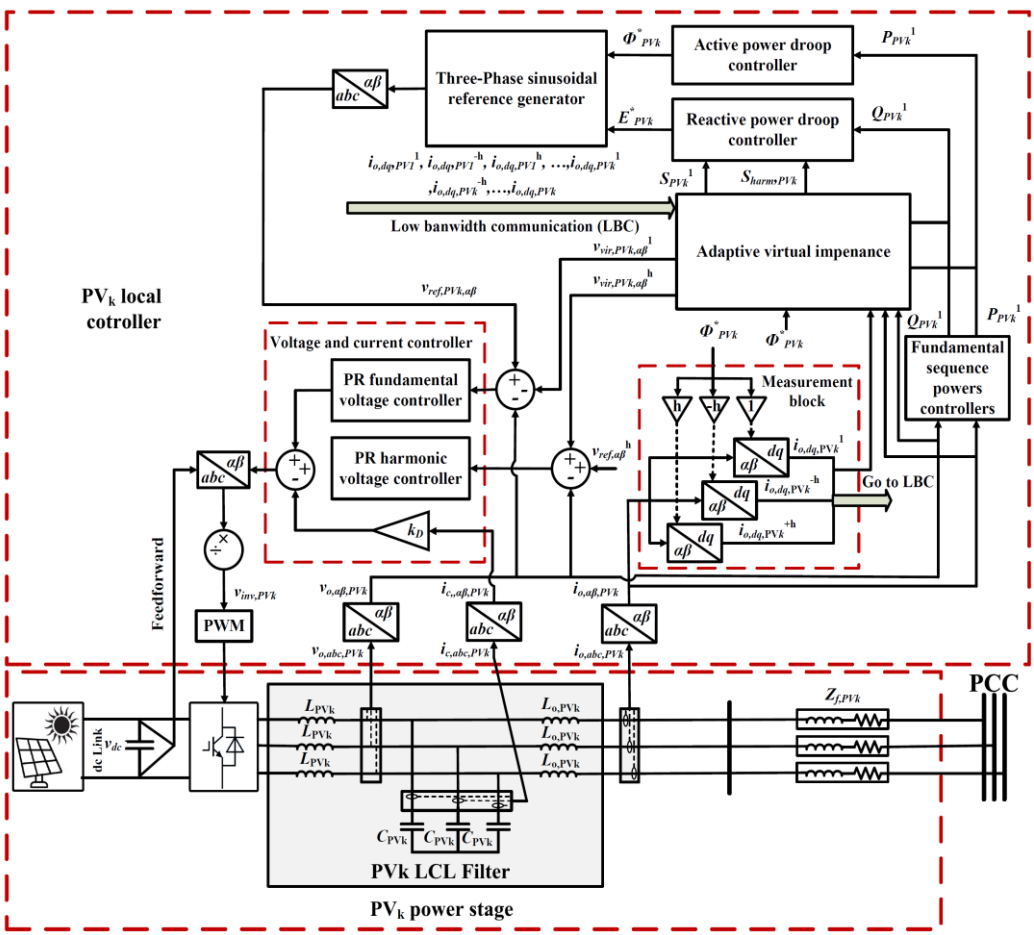

Figure 2. The power stage and local control structures of PV inverters with LCL filter.

2.1. Modified droop controllers for active and reactive power

The active and reactive power outputs of each PV in a predominantly inductive system can be controlled by regulating its output frequency and voltage amplitude, respectively. Based on this principle, the $P-\omega$ and $Q-E$ droop controllers, as defined in the following equations, can be used to distribute active and reactive power among the DGs in an islanded MG [35]. Figure 3 illustrates the behavior of these droop controllers. As shown, by adjusting the slope of these controllers, the active and reactive power outputs of the PVs can be effectively managed.

$$\omega^{*}_{PVk} = \omega_{0,PVk} - m_p.P^{1}_{PVk} \quad (1)$$

$$E^{*}_{PVk} = E_{0,PVk} - n_q.Q^{1}_{PVk} \quad (2)$$

where $\omega_{0,PVk}$ and $E_{0,PVk}$ represent the nominal values of the angular frequency and output voltage amplitude of the PV. $\omega_{PVk}{}^{*}$ and $E_{PVk}{}^{*}$ denote the reference values of frequency and voltage amplitude. The coefficients m_p and n_q determine the slopes of the droop controllers for active and reactive power, respectively. These coefficients are calculated based on the following equations.

$$m_p = \frac{\Delta\omega_{\mathrm{PVk,max}}}{P_{\mathrm{PVk,max}}} \quad (3)$$

$$n_q = \frac{\Delta E_{\mathrm{PVk,max}}}{Q_{\mathrm{PVk,max}}} \quad (4)$$

where $P_{PVk,max}$ and $Q_{PV,max}$ represent the maximum active and reactive power that can be generated by each PV unit, and $\Delta\omega_{PVk,\mathrm{max}}$, $\Delta E_{PVk,\mathrm{max}}$ denote the maximum allowable deviations of frequency and voltage of the MG PVs from their nominal values.

In [36], it is highlighted that phase-based droop controllers outperform frequency-based droop controllers due to a key limitation: the minimum allowable frequency restricts the slope of frequency-based droop controllers (m_p in equation (1)). This limitation reduces the accuracy of power sharing among PVs. Moreover, the phase angle of the output voltage can be easily adjusted with changes in load. Therefore, in this paper, the active power droop controller introduced in equation (5) is used instead of the droop controller in equation (1).

$$\varphi^{*}_{PV,k} = \varphi_{0,PVk} - (m_{pp} + \frac{m_{ip}}{s}).P^{1}_{PVk} \quad (5)$$

where $\phi_{0,PVk}$ is the nominal phase angle, m_{pp} and m_{ip} are the proportional and integral coefficients for active power, respectively. $\phi_{PVk}{}^{*}$ represents the reference phase angle of the output voltage, and s is the Laplace variable.

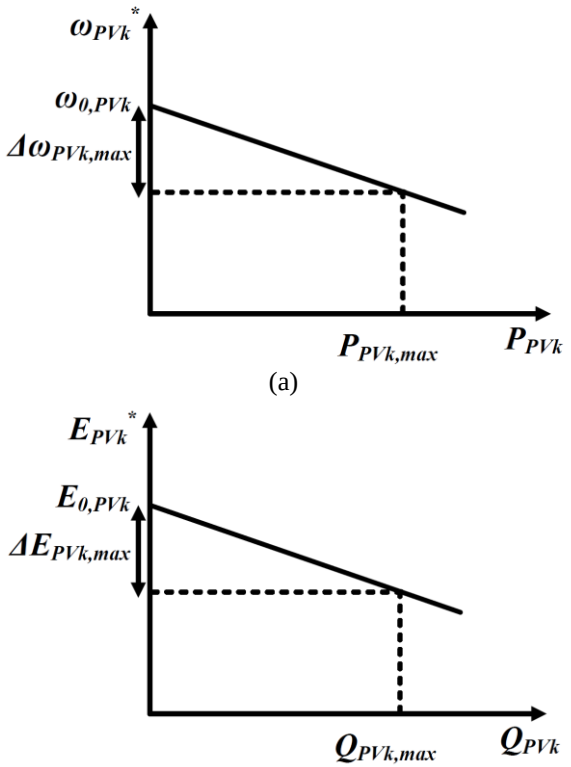

Figure 3. Active and reactive droop controller, (a) $P-\omega$, (b) $Q-E$

In steady-state operation, the frequency of all PVs synchronizes to the same value. Additionally, due to the relationship between frequency and voltage angle, the voltage angles of all PVs quickly adjust relative to one another. This process ultimately results in equal active power generation by the PVs and ideal active power sharing within the MG. However, since the voltage amplitude droop of PVs is affected by the differing impedances of their feeders, the output voltage amplitudes of the PVs are not equal. Consequently, reactive power is not properly shared among the sources. Therefore, the $Q-E$ droop control introduced in equation (1) needs to be modified, as explained in the following sections.

In an MG with nonlinear loads, the harmonic components of voltage and current can occupy the capacity of the interfacing inverters of the PVs. According to the IEEE 1459-2010 standard [37], the total power supplied by each DG can be calculated as follows:

$$S_{PVk} = \sqrt{(S^{1}_{PVk})^2 + (S_{harm,PVk})^2} \quad (6)$$

$$S^{1}_{PVk} = \sqrt{(P^{1}_{PVk})^2 + (Q^{1}_{PVk})^2} \quad (7)$$

where S_{PVk}^1 is the fundamental apparent power and $S_{harm,PVk}$ is the harmonic apparent power, which is calculated as follows:

$$S_{harm,PV}k = S_{PVk}^1 . \sqrt{(THD_I)^2 + (THD_V)^2} \quad (8)$$

$$THD_v = \frac{\sqrt{(v_d^{oc})^2 + (v_q^{oc})^2}}{\sqrt{(v_d^1) + (v_q^1)^2}} \quad (9)$$

$$THD_I = \frac{\sqrt{(i_d^{oc})^2 + (i_q^{oc})^2}}{\sqrt{(i_d^1) + (i_q^1)^2}} \quad (10)$$

where THD_I and THD_V represent the total harmonic distortion of the output current and voltage of the PV, respectively.

According to the presented equations, the maximum reactive power injected by the PVs can be calculated as follows. As observed, the maximum reactive power of the PVs depends not only on their rated power and active power but also on their harmonic power.

$$Q_{\mathrm{PVk,max}} = \sqrt{(S_{PVk})^2 - (P_{PVk}^1)^2 - (S_{harm,PVk})^2} \quad (11)$$

By substituting equation (11) into equation (4), the reactive power droop coefficients of the PVs can be calculated as follows:

$$n_q = \frac{\Delta E_{\mathrm{PVk,max}}}{Q_{\mathrm{PVk,max}}} = \frac{\Delta E_{PVk,\max}}{\sqrt{(S_{PVk})^2 - (P_{PVk}^1)^2 - (\mathrm{S_{harm,PVk}})^2}} \quad (12)$$

By substituting equation (12) into equation (2), the reactive power droop characteristic is modified as follows:

$$E_{PVk}^* = E_{0,PVk} - \frac{\Delta E_{PVk,\max}}{\sqrt{(S_{PVk})^2 - (P_{PVk}^1)^2 - (\mathrm{S_{harm,PVk}})^2}} Q_{PVk}^1 \quad (13)$$

As observed in equation (13), if the voltage deviation is high, the PV will contribute more to supplying reactive power, thereby improving reactive power sharing within the MG and preventing the overloading of PV inverters.

2.2. The Proposed Adaptive VI Structure

In an islanded MG, the asymmetry in the output impedance of PV inverters significantly impacts the accuracy of sharing fundamental and harmonic current components. Although utilizing droop controlllers for active and reactive power enhances the sharing of the fundamental component of the load current, asymmetry causes these controllers to perform undesirably. Moreover, due to component tolerances and variations in the switching patterns of inverters, circulating fundamental and harmonic currents are automatically generated among the PV inverters. Furthermore, the asymmetry of MG impedances increases circulating currents, which in turn leads to improper sharing of both the fundamental and harmonic powers among the PVs. Effectively controlling circulating currents is essential to maintain the stability of the islanded MG, prevent overloading of certain inverters, and improve the quality of load sharing among the PVs.

According to figure 2, an *LCL* filter is used at the output of the PV inverter. The *LCL* filter consists of an *LC* filter section and an output inductor $L_{o,PV}$. The use of $L_{o,PV}$ helps reduce circulating currents among the PV inverters. However, if the voltage and current controllers are designed appropriately to limit the disturbances in the output voltage of the LC filter, the disturbance-induced voltage drop across $L_{o,PV}$ (caused by harmonic currents) will result in voltage distortion after the inductor. Such distortion adversely affects the performance of the PV inverters.

The proposed adaptive VI structure, shown in figure 4, consists of two parts. In the first part, a resistive-inductive VI is employed to enhance the performance of droop controllers for active and reactive power and to reduce the circulating currents of the fundamental component of the load current. In the second part, resistive-capacitive VIs are used to improve the harmonic components sharing of the load current, reduce the circulating currents of the harmonic components, and enhance the output voltage quality of the PV inverters. The operation of the proposed VI is described by the following equations.

$$v_{av\alpha,PVk}^1 = R_{vir}^1 . i_{cir,o\alpha,PVk}^1 - \omega_0 L_{vir}^1 . i_{o\beta,PVk}^1 \quad (14)$$

$$v_{av\beta,PVk}^1 = R_{vir}^1 . i_{cir,o\beta,PVk}^1 + \omega_0 L_{vir}^1 . i_{o\alpha,PVk}^1 \quad (15)$$

$$v_{av\alpha,PVk}^{+h} = R_{vir}^h . i_{cir,o\alpha,PVk}^{+h} + h\omega_0 L_{o,\mathrm{PVk}}^{+h} . i_{o\beta,PVk}^{+h} \quad (16)$$

$$v_{av\beta,PVk}^{+h} = R_{vir}^h . i_{cir,o\beta,PVk}^{+h} - h\omega_0 L_{o,\mathrm{PVk}}^{+h} . i_{o\alpha,PVk}^{+h} \quad (17)$$

$$v_{av\alpha,PVk}^{-h} = R_{vir}^h . i_{cir,o\alpha,PVk}^{-h} - h\omega_0 L_{o,\mathrm{PVk}}^{-h} . i_{o\beta,PVk}^{-h} \quad (18)$$

$$v_{av\beta,PVk}^{-h} = R_{vir}^h . i_{cir,o\beta,PVk}^{-h} + h\omega_0 L_{o,\mathrm{PVk}}^{-h} . i_{o\alpha,PVk}^{-h} \quad (19)$$

where L_{vir}^1 represents the virtual inductance for inductivizing the output impedance of PVs, $R_{vir}^1$and R_{vir}^h are the virtual resistances for the fundamental and harmonic components, respectively. $i_{cir,o\alpha\beta}^1$ and $i_{cir,o\alpha\beta}^h$ denote the circulating currents of the fundamental and harmonic components of the PV output, respectively. $L_{o,PVk}^{+h}$ and $L_{o,PVk}^{-h}$ are the virtual capacitive impedances for the harmonic components, and ω is the system frequency. The virtual capacitive impedances reduce the harmonic voltage drops generated at the output of LCL filters by introducing an inductive impedance of magnitude

$-L_{o,PVk}$. Moreover, instead of ω_0, $+h\omega_0$ is used for the *7th*-order harmonic (positive sequence), and $-h\omega_0$ is applied for the *5th*-order harmonic (negative sequence). The circulating currents among multiple parallel PV inverters are defined by the following equations, representing the difference between the actual output current and the allocated load current.

$$i^{1}_{Cir,odq,\mathrm{PV}k} = i^{1}_{odq,\mathrm{PV}k} - D_k \sum_{k=1}^{N} i^{1}_{o,dq,\mathrm{PV}k} \tag{20}$$

$$i^{\pm h}_{Cir,odq,\mathrm{PV}k} = i^{\pm h}_{odq,\mathrm{PV}k} - D_k \sum_{k=1}^{N} i^{\pm h}_{o,dq,\mathrm{PV}k} \tag{21}$$

where D_k is the load distribution factor, which is proportional to the rated power of the PVs. D_k can be calculated using the following equation [33]:

$$D_k = \frac{S_{0,\mathrm{PV}k}}{S_T} = \frac{S_{0,\mathrm{PV}k}}{\sum_{k=1}^{N} S_{0,\mathrm{PV}k}} \tag{22}$$

where $S_{0,PVk}$ and S_T represent the rated power of $\mathrm{PV_k}$ and the total loading capacity of the PVs, respectively.

According to figure 4 and equations (14-19), the resistances $R_{vir}{}^{1}$ and $R_{vir}{}^{h}$ are used to improve the sharing of active and reactive powers and harmonic power of the load among the PVs, as well as to reduce circulating currents between them. The $R_{vir}{}^{h}$ is specifically designed for the dominant harmonic circulating currents. As observed, unlike previous VI designs where virtual resistances were placed in the path of the total current, these resistances are positioned in the path of the circulating currents. This approach prevents additional voltage drops at the output of the PV inverters. The value of $R_{vir}{}^{h}$ is adaptively calculated based on the nonlinear load supplied by each PV, as shown in the following equation:

$$R^{h}_{vir} = k_{hp}.S_{harm,\mathrm{PVk}} \tag{23}$$

In the above equation, as $S_{harm,PVk}$ increases, the value of $R_{vir}{}^{h}$ also increases. This increase acts as a limiting factor for $S_{harm,PVk}$ because higher $R_{vir}{}^{h}$ reduces the harmonic circulating currents of $\mathrm{PV_k}$. Consequently, excessive nonlinear load sharing by any single PV is prevented, and nonlinear load sharing is performed proportionally. k_{ph} is a positive constant gain determined based on the rated power distribution among the PVs.

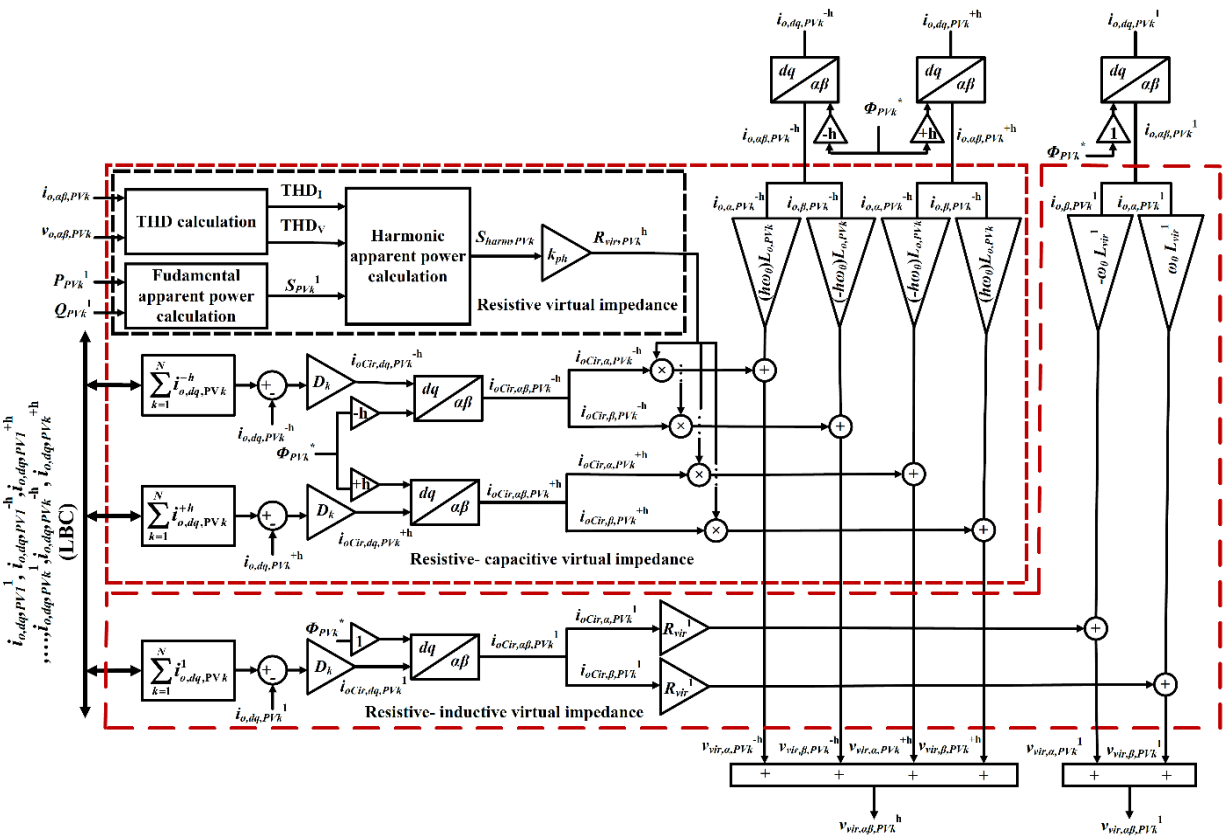

Figure 4. Proposed Adaptive VI Structure.

3. Determination of Control System Parameters for PV Inverters

In figure 2, two separate voltage control loops are utilized to manage the fundamental and harmonic components of the voltage. Additionally, a k_D control loop is implemented to improve the damping performance and dynamic response of the PV system. This loop utilizes feedback from the current of the LCL filter capacitor [7]. By deriving the closed-loop transfer functions for the reference voltages of the fundamental ($f_{CL}^{1}(s)$) and harmonic components ($f_{CL}^{h}(s)$), as well as the equivalent closed-loop output impedance of the control system ($Z_0(s)$), the parameters of the control system for PV inverters can be optimized. These functions are represented by the following equations:

$$f_{CL}^{1}(s) = \frac{f_v^{1}(s).f_{PWM}(s) + Z_2(s)}{f_{PWM}(s)Z_2(s).(f_v^{1}(s) + f_v^{h}(s)) + f_{PWM}(s).K_D + Z_1(s) + Z_2(s)} \quad (24)$$

$$f_{CL}^{h}(s) = \frac{f_v^{h}(s).f_{PWM}(s).Z_2(s)}{f_{PWM}(s)Z_2(s)(f_v^{1}(s) + f_v^{h}(s)) + f_{PWM}(s).k_D + Z_1(s) + Z_2(s)} \quad (25)$$

$$Z_0(s) = \frac{Z_2(s)}{f_{PWM}(s).Z_2(s).(f_v^{1}(s) + f_v^{h}(s)) + f_{PWM}(s).k_D.Z_2(s) + Z_2(s)} \quad (26)$$

$$f_{PWM} = \frac{1}{1+1.5T_s.s} \quad (27)$$

$$Z_1(s) = L_{PVk} + r_{PVk} \quad (28)$$

$$Z_2(s) = \frac{1}{sC_{PVk}} \quad (29)$$

where $f_v^{1}(s)$ and $f_v^{h}(s)$ represent the functions of the fundamental and harmonic voltage controllers, respectively. Z_1 and Z_2 denote the output impedances of the PV inverter's output filter, f_{PWM} is the transfer function of the PWM block, and T_s is the sampling time.

The Bode diagrams of $f_{CL}^{1}(s)$ and $f_{CL}^{h}(s)$, generated using the parameters provided in Table 1, are shown in figure 5. As observed, the magnitude and phase angle of $f_{CL}^{1}(s)$ at the fundamental frequency (50Hz) are 1 and 0, respectively, while the magnitude at the dominant harmonic frequencies (250Hz for the *5th* harmonic and 350Hz for the *7th* harmonic) is approximately zero. Similarly, this description can be applied to the Bode diagram of $f_{CL}^{h}(s)$. Figure 6 depicts the Bode diagram of $Z_0(s)$. As shown, the output impedance magnitude of the PV inverter at frequencies of 50Hz, 250Hz, and 350Hz is nearly zero. Therefore, based on the presented analysis, it can be concluded that the fundamental voltage reference is effectively tracked without interference from the harmonic voltage reference tracking loop.

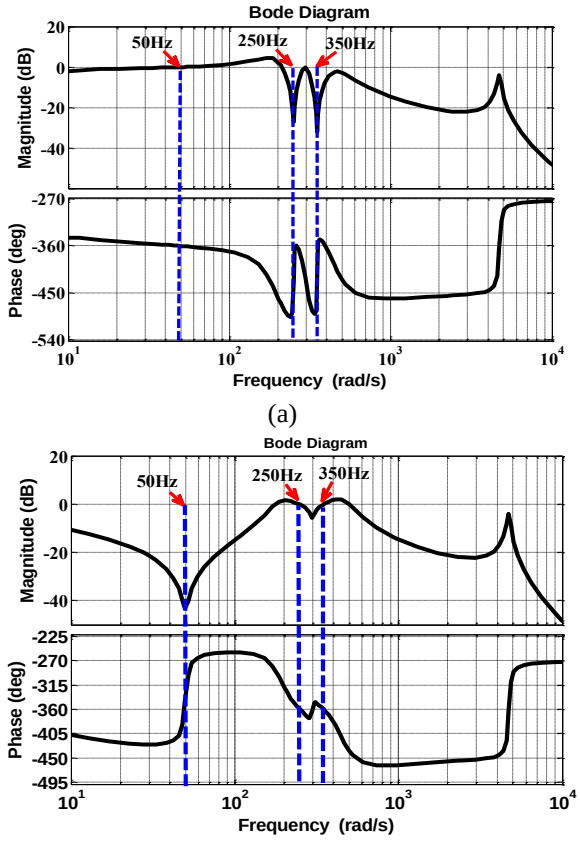

Figure 5. The Bode diagrams of the closed-loop transfer functions, (a) $f_{CL}^{1}(s)$, (b) $f_{CL}^{h}(s)$

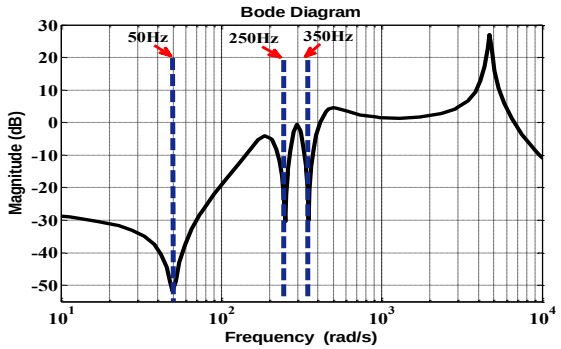

Figure 6. The bode diagram of the equivalent closed-loop output impedance of the PV Inverter.

4. Simulation Results

In figure 7, the schematic diagram of the studied islanded MG is shown. This MG consists of three PV units connected to the PCC through LCL filters. The inverter control system of the PV units operates locally and communicates via LBC. The nominal capacities of the PV units are specified as $S_{PV1}=S_{PV2}=2S_{PV3}$. The nominal voltage and frequency of the MG are 230V and 60Hz, respectively. At the PCC, a three-phase full-bridge diode rectifier is used as a nonlinear load, along with a balanced star-connected linear load. It is important to note that compensation has been performed for dominant voltage and current harmonics (5th and 7th order harmonics). Additionally, a communication delay of 1ms for the LBC is considered in the simulation. The parameters of the control system and PV power stage are provided in Table1. As observed, the distribution line impedances of the PV units are chosen such that an asymmetrical MG is achieved ($Z_{f,PV1}=Zf_{,PV2}=2Z_{f,PV3}$). The simulation is carried out in the MATLAB/Simulink environment. To validate the effectiveness of the proposed method, the simulation is performed in four steps, as outlined below:

- In the first step (0sec≤t<2sec), the conventional *P-ϕ* and *Q-E* droop controllers and the virtual inductances of the fundamental components are activated.
- In the second step (2sec≤t<3.5sec), modified *Q-E* droop controllers and virtual resistances of the fundamental components are activated.
- In the third step (3.5sec≤t<5sec), the adaptive virtual resistances of the fundamental and harmonic components are activated.
- In the fourth step (5sec≤t<6.5sec), the virtual capacitors are activated for voltage harmonic compensation.

4.1. First step (0sec≤t<2sec)

In figure 8, the output voltages of the PVs (at the output of the *LC* filters) during different simulation steps are shown. As expected, in the first step, the output voltages of the PVs are almost undistorted. This is reflected in Table 2, where the very low *THD* values of the output voltage for all PVs demonstrate the effectiveness of the voltage controllers in tracking the reference voltage despite the presence of a nonlinear load. However, Table 2 also indicates that due to the harmonic voltage drop across the output inductance of the *LCL* filters ($L_{o,PVk}$) and the feeder impedances of the PVs, the THD of the PCC voltage is significantly high.

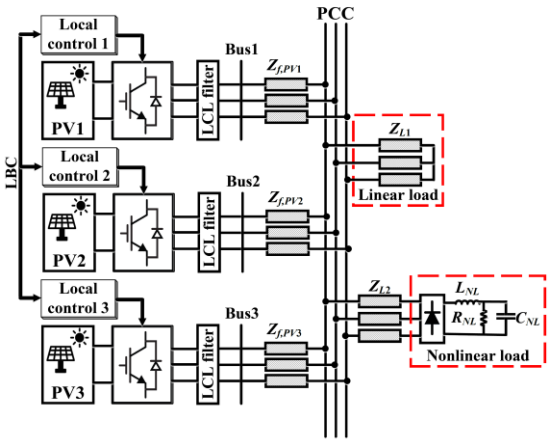

Figure 7. Th.e schematic diagram of the studied islanded MG

Tabele 1. Control system parameters and the power section of the MG

Rate pawer of PVs					
S_{PV1} (kVA)		S_{PV2} (kVA)		S_{PV3} (kVA)	
5		5		2.5	
Droop controllers of fundamental active power (PV_1, PV_2 and PV_3)					
$m_{pp,1}$ (rad/W)	$m_{pp,2}$ (rad/W)	$m_{pp,3}$ (rad/W)	$m_{ip,1}$ (rad/W)	$m_{i,2}$ (rad/W)	$m_{ip,3}$ (rad/W)
2×10^{-5}	2×10^{-5}	4×10^{-5}	2×10^{-4}	2×10^{-4}	4×10^{-4}
Resistive-indactive virtual impedances					
$R_{vir,1}{}^1$ (Ω)	$L_{vir,1}{}^1$ (mH)	$R_{vir,2}{}^1$ (Ω)	$L_{vir,2}{}^1$ (mH)	$R_{vir,3}{}^1$ (Ω)	$L_{vir,3}{}^1$ (mH)
0.25	2.5	0.25	2.5	5	0.5
Resistive-capacitive virtual impedances					
$k_{hp,1}$	$k_{hp,2}$	$k_{hp,3}$	$L_{o,PV1}$ (mH)	$L_{o,PV1}$ (mH)	$L_{o,PV1}$ (mH)
0.02	0.02	0.04	1.8	1.8	1.8
Voltage and current conrollers						
k_D	$k_{pv}{}^1$	$k_{pv}{}^5$	$k_{pv}{}^7$	$k_{rV}{}^1$	$k_{rV}{}^5$	$k_{rV}{}^7$
0.2	1	5	5	1200	600	800
LCL filters						
LCL_{PV1} (mH, μF, mH)		LCL_{PV2} (mH, μF, mH)		LCL_{PV3} (mH, μF, mH)	
1.8, 25, 1.8		1.8, 25, 1.8		1.8, 25, 1.8	
PVs feeder impedance					
$Z_{f,PV1}$ (Ω, mH)		$Z_{f,PV1}$ (Ω, mH)		$Z_{f,PV1}$ (Ω, mH)	
0.2-2.6		0.3-3.8		0.1-1.3	
Linear and nonlinear loads					
Z_{L1} (Ω, mH)	R_{NL} (Ω)		L_{NL} (mH)	C_{NL} (μF)	
50, 20	150		0.084	235	

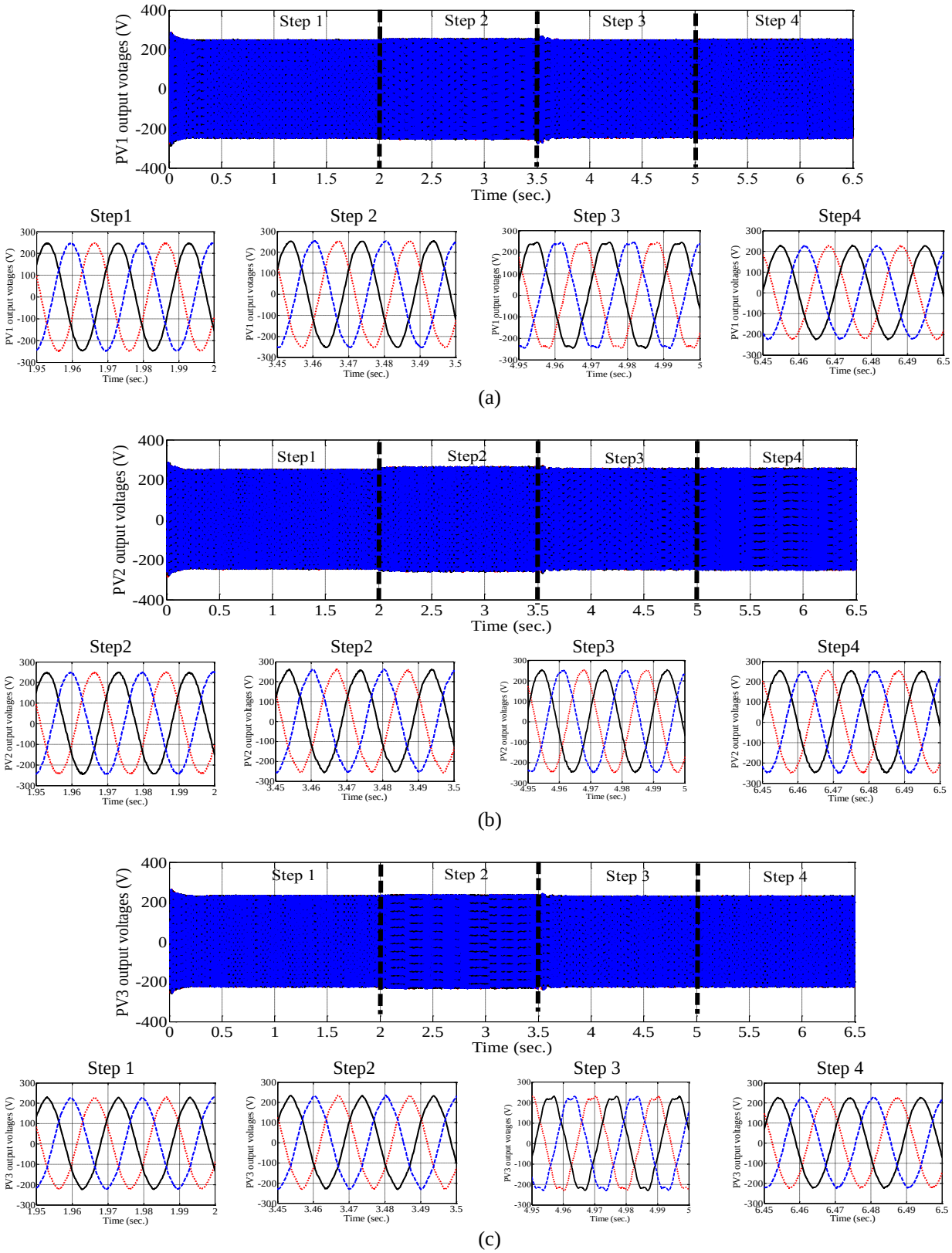

Figure 8. The output voltage waveform of the PVs. (a) PV_2, (b) PV_1, (c) PV_3,

Table 2. THD values of output voltages of PV units and PCC in different simulation steps

	THD (%)			
	$v_{C,PV1}$	$v_{C,PV2}$	$v_{C,PV3}$	v_{PCC}
First step	0.42	0.41	0.37	2.21
Second step	0.43	0.42	0.38	2.32
Third step	1.92	2.33	1.32	3.32
Fourth step	0.74	1.12	0.52	1.13

Figure 9 illustrates the active and reactive power sharing of the fundamental component among all PVs under different simulation steps. As shown in figure 9a, despite the asymmetry in the feeder impedances of the PVs, the fundamental active power is shared proportionally to the rated capacity of the PVs. Therefore, it can be concluded that the droop controllers for active power exhibit satisfactory performance. However, as observed in figure 9b, due to the asymmetry in the feeder impedances of the PV units, there is a significant error in the reactive power sharing of the fundamental component among the PVs relative to their rated capacities. Thus, it can be inferred that conventional droop controllers for reactive power (equation (2)) do not perform adequately in sharing the fundamental reactive power among the PV units. figure 10 presents the three-phase output currents of the PVs. As observed, due to the asymmetry in the feeder impedances of the PVs, the magnitudes of the output currents are not proportional to the rated capacities of the PVs.

4.2. Second step (2sec≤t<3.5sec)

In the second simulation step, the modified droop controller and the virtual resistances of the fundamental component are activated. As shown in equation 13 and figure 9, by adjusting the slope of the reactive power droop control based on the remaining capacity of the interfacing inverters, the reactive power sharing among the PVs significantly improves in the second step. However, it is still not proportional to the rated capacities of the PVs. This is also evident in figure 10, where the three-phase output currents of the PVs are depicted. As observed, the output current magnitudes of the PVs are improved to better align with their rated capacities. Figures 11 and 12 illustrate the dominant harmonic currents (*5th* and *7th* order harmonics) of the PV outputs for phase "*a*". As shown, in the second step, before the activation of the harmonic virtual resistances, the output current magnitudes (step 2 in figure 10) are not proportional to the PV capacities due to improper sharing of harmonic currents among the PVs. Figure 13 depicts the circulating harmonic currents of the *5th* and *7th* orders in phase "*a*". As observed, during this step, due to the asymmetry in the feeder impedances of the PVs and the improper sharing of load harmonic currents, circulating harmonic currents flow among the PV inverters.

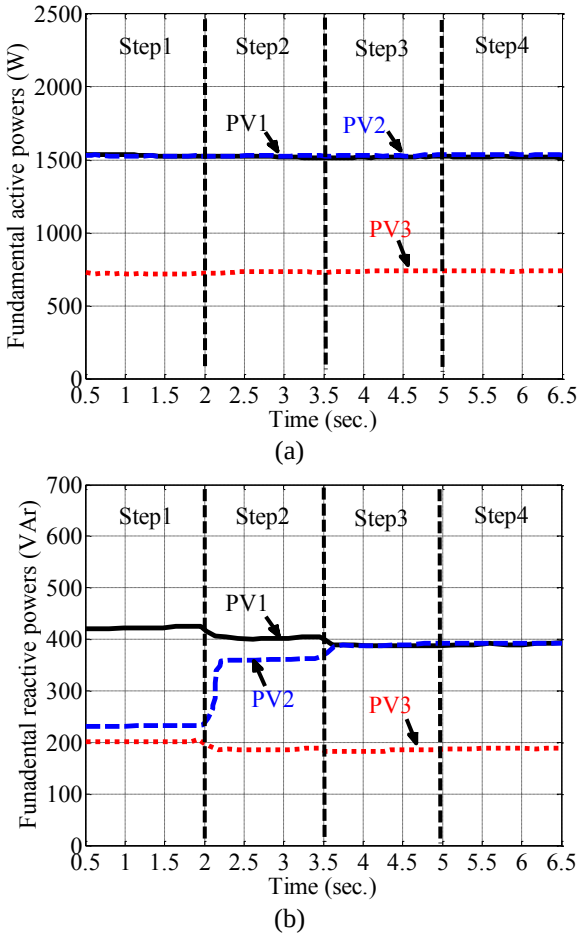

Figure 9. Fundamental component powers of PV units, (a) active power, (b) reactive power

4.3. Third step (3.5sec≤t<5sec)

In the third step, adaptive virtual resistances for both the fundamental and harmonic components are activated to improve the sharing of fundamental and harmonic load currents among the PVs. As shown in figure 9b, the introduction of the fundamental virtual resistances improves the reactive power sharing among the PV units. In figures 11b and 12b, it is evident that with the activation of these resistances, the sharing of harmonic load currents among the PVs improves in proportion to their rated capacities (the harmonic load currents supplied by PV_1 and PV_2 are approximately double those supplied by

PV_3). This improvement is also observable in figure 10, which depicts the three-phase output currents of the PVs. Moreover, according to Figure 8 and Table 2, in this step, the addition of load current sharing loops at harmonic frequencies results in increased voltage distortion at the PV outputs and subsequently at the PCC. However, as observed, unlike conventional harmonic virtual impedance schemes, the effect of adaptive harmonic resistances on increasing the output distortion of PV units is lower. This result can be explained by the fact that the proposed adaptive virtual resistances are placed in the feedback path of the circulating currents for dominant harmonic components. This is clearly reflected in Table 2, where the THD values of the PV output voltages remain within an acceptable range, below 2.5%, in compliance with IEEE standards [38]. Figure 13 further illustrates that with the activation of adaptive virtual resistances, the circulating harmonic currents are significantly reduced, indicating effective harmonic current sharing among the PVs.

4.4. fourth step (3.5sec≤t<5sec)

In this step, virtual capacitors are activated at t=5s. According to the results in Table 2, it is observed that with the introduction of virtual capacitive impedances, the THD of the PV output voltages and the PCC voltage are significantly reduced due to the compensation of harmonic voltage drops across $L_{o,\mathrm{PVk}}$. The improvement in the voltage quality of the PV outputs and the PCC is also evident in figures 8.

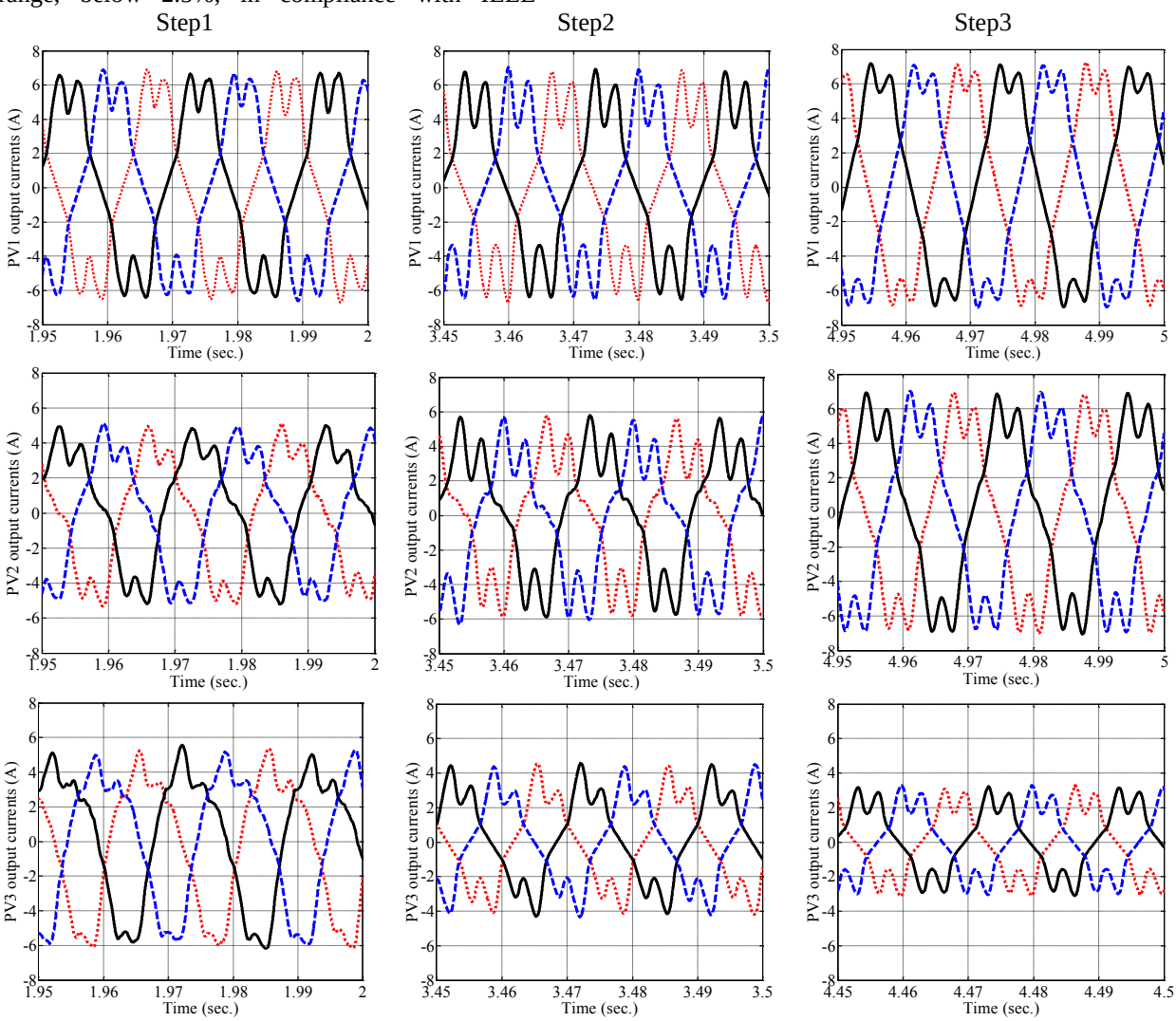

Figure 10. Three-Phase Output Current Waveforms of PV Units, row 1: PV_1, row 2: PV_2, row 3: PV_3

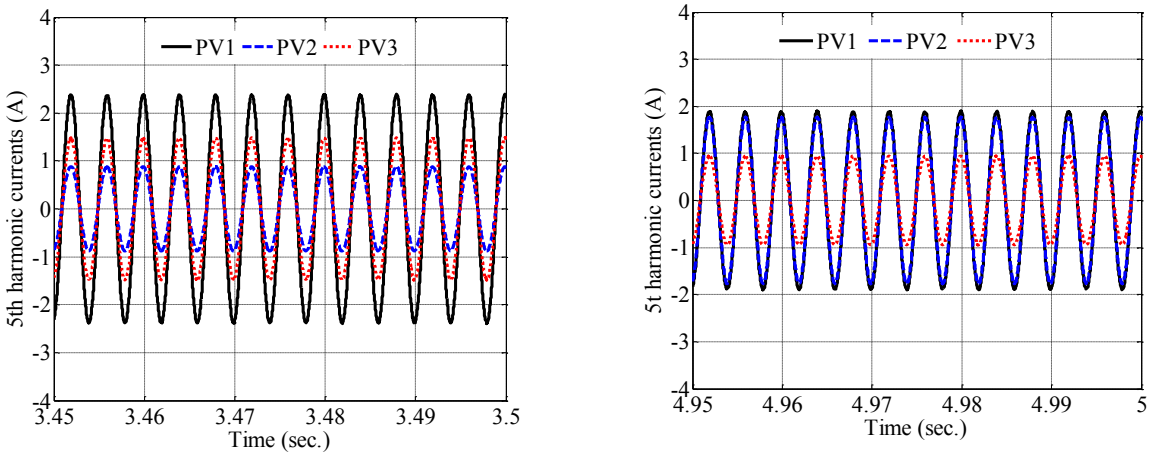

Figure 11. *5th* harmonic component of phase "*a*" output current, (a) step 2, (b) step 3

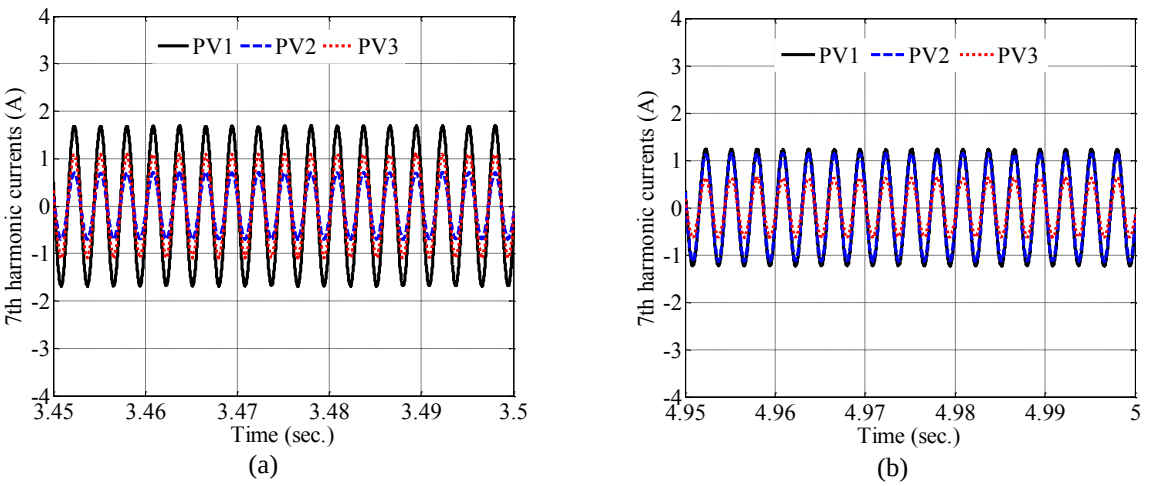

Figure 12. *7th* harmonic component of phase "*a*" output current, (a) step 2, (b) step 3

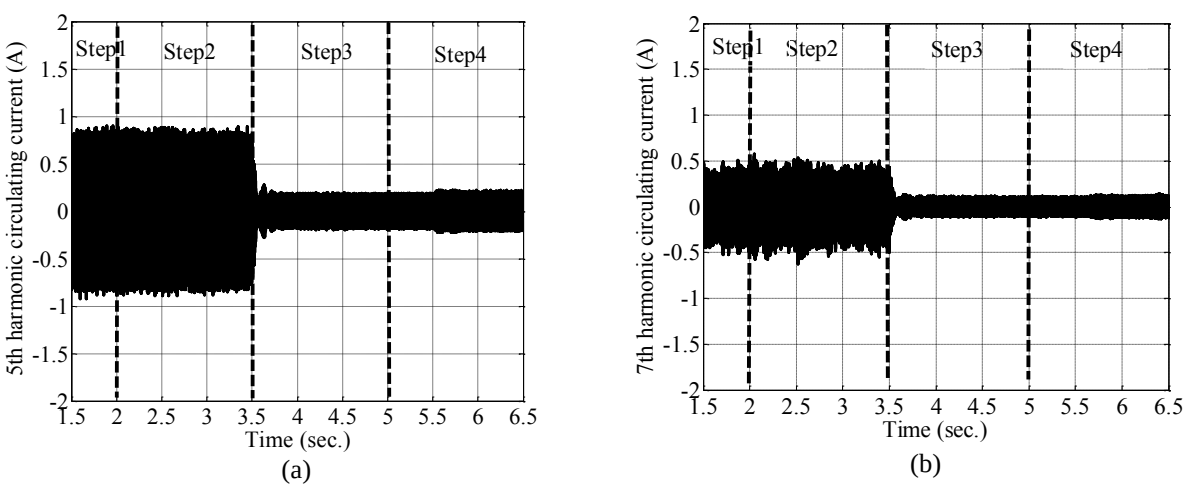

Figure 13. harmonic components of circulating current in phase "*a*", (a) *5th* harmonic component, (b) *7th* harmonic component

5. Conclusion

In this paper, a local control structure is proposed for PV inverters with *LCL* filters. The objective of this control scheme is to compensate for PCC voltage distortion and improve the sharing of the fundamental and harmonic components of load currents among PV units. The proposed structure employs modified droop controllers to enhance the reactive power sharing of the fundamental component. The slopes of these controllers are determined based on the remaining capacity of the PV units. As a result, reactive power sharing among PV units is improved, and overloading of interfacing inverters due to reactive power compensation is prevented. Additionally, an adaptive virtual impedance scheme is proposed in this structure. Adaptive virtual resistances are utilized to enhance the sharing of both fundamental and harmonic components of the load current based on the circulating current principle. It is demonstrated that the designed virtual resistances can improve the sharing of these load current components without requiring knowledge of the MG topology, such as the impedances of PV distribution lines. Moreover, the impact of the proposed scheme on the magnitude and quality of the PV output voltage waveforms is minimal. This advantage arises because the compensation loops are applied only to the circulating components of the fundamental and harmonic currents rather than the entire load current path. Furthermore, the quality of the *LCL* filter output voltage is critical, as sensitive loads may be connected at the output of the *LCL* filter. To address this, the proposed structure employs virtual capacitors to enhance the LCL filter's output voltage quality. Simulation results demonstrate that the proposed local control structure can effectively improve the output voltage quality of PVs and enhance the sharing of fundamental and harmonic components of load currents among PV inverters, proportional to their rated capacities. In the next step, our focus will be on refining the droop control structure for reactive power and VI to improve voltage unbalance compensation in islanded MGs operating with nonlinear and unbalanced loads.

Nomenclature

DG	Distributed generation
D_k	Load distribution factor
$E_{0,PVk}$	Nominal values of output voltage amplitude of the PV_k
E_{PVk^*}	Reference values of voltage amplitude
$f_{CL}^1(s)$	Closed-loop transfer functions for the fundamental reference voltage
$f_{CL}^h(s)$	Closed-loop transfer functions for the harmonic reference voltage
f_{PWM}	Transfer function of the PWM
$f_v^1(s)$	Functions of the fundamental voltage controller
$f_v^h(s)$	Functions of the harmonic voltage controller
$i_{cir,o\alpha\beta}^1$	Fundamental circulating current
$i_{cir,o\alpha\beta}^h$	Harmonic circulating currents
LBC	Low-bandwidth communication
L_{vir}^1	Virtual inductance
MG	Microgrid
m_{ip}	The integral coefficient for active power
m_p	The slopes of the droop controller for active power
m_{pp}	The proportional coefficient for active power
n_q	The slope of the droop controller for reactive power
PCC	Point of common coupling
$P_{PVk,max}$	Maximum active power of PV_k
PR	Proportional-resonant
$Q_{PV,max}$	Maximum reactive power of PV_k
R_{vir}^1	Fundamental virtual resistance
R_{vir}^h	Harmonic virtual resistances
s	Laplace variable
$S_{0,PVk}$	The rated power of PV_k
$S_{harm,PVk}$	Harmonic apparent power
S_{PVk}^1	Fundamental apparent power
S_T	The total loading capacity of the PVs
THD_I	Total harmonic distortion of the current
THD_V	Total harmonic distortion of the voltage
T_s	Sampling time
VI	Virtual impedance
$Z_0(s)$	Closed-loop output impedance of the control system
$\Delta E_{PVk,\max}$	Maximum allowable deviation of voltage of the MG PVs
$\Delta\omega_{PVk,max}$	Maximum allowable deviation of Frequency of the MG PVs
$\phi_{0,PVk}$	Nominal phase angle
ϕ_{PVk^*}	Reference phase angle of the output voltage

ω	System frequency
$\omega_{0,PVk}$	Nominal values of the angular frequency of the PV_k
ω_{PVk^*}	Reference values of frequency

References

[1] Liserre, M., Sauter, T., Hung, J. Y. (2010). Future energy systems: Integrating renewable energy sources into the smart power grid through industrial electronics. *IEEE Industrial Electronics Magazine*, *4*(1), 18-37. https://doi.org/10.1109/MIE.2010.935861

[2] Wang, K., Yuan, X., Geng, Y., Wu, X. (2019). A practical structure and control for reactive power sharing in microgrid. *IEEE Transactions on Smart Grid*, *10*(2), 1880-1888. https://doi.org/10.1109/TSG.2017.2779846

[3] IEEE Standard 1547.4-2011. (2011). IEEE guide for design, operation, and integration of distributed resource island systems with electric power systems. https://doi.org/10.1109/IEEESTD.2011.5960751

[4] Lee, T. L., & Hu, S. H. (2011). Resonant current compensator with enhancement of harmonic impedance for LCL-filter based active rectifiers. *IEEE Applied Power Electronics Conference and Exposition (APEC)*, 1538-1543. https://doi.org/10.1109/APEC.2011.5744798

[5] Moussa, H., Shahin, A., Martin, J. P., Nahid-Mobarakeh, B., Pierfederici, S., & Moubayed, N. (2018). Harmonic power sharing with voltage distortion compensation of droop controlled islanded microgrids. *IEEE Transactions on Smart Grid*, *9*(5), 5335-5347. https://doi.org/10.1109/TSG.2017.2687058

[6] Sreekumar, P., & Khadkikar, V. (2017). Direct control of the inverter impedance to achieve controllable harmonic sharing in the islanded microgrid. *IEEE Transactions on Industrial Electronics*, *64*(1), 827-837. https://doi.org/10.1109/TIE.2016.2574308

[7] Lorzadeh, I., Abyaneh, H. A., Savaghebi, M., & Guerrero, J. M. (2015). A hierarchical control scheme for reactive power and harmonic current sharing in islanded microgrids. *17th European Conference on Power Electronics and Applications (EPE'15 ECCE-Europe*, 1-10. https://doi.org/10.1109/EPE.2015.7311770

[8] Mahmood, H., Michaelson, D., & Jiang, J. (2015). Accurate reactive power sharing in an islanded microgrid using adaptive virtual impedances. *IEEE Transactions on Power Electronics*, *30*(3), 1605-1617. https://doi.org/10.1109/TPEL.2014.2314721

[9] Han, H., Liu, Y., Sun, Y., Su, M., & Guerrero, J. M. (2015). An improved droop control strategy for reactive power sharing in islanded microgrid. *IEEE Transactions on Power Electronics*, *30*(6), 3133-3141. https://doi.org/10.1109/TPEL.2014.2332181

[10] Tuladhar, A., Jin, H., Unger, T., & Mauch, K. (2000). Control of parallel inverters in distributed AC power systems with consideration of line impedance effect. *IEEE Transactions on Industry Applications*, *36*(1), 131-138. https://doi.org/10.1109/28.821807

[11] Pham, M. D., & Lee, H. H. (2021). Effective coordinated virtual impedance control for accurate power sharing in islanded microgrid. *IEEE Transactions on Industrial Electronics*, *68*(3), 2279-2288. https://doi.org/10.1109/TIE.2020.2972441

[12] Hoang, T. V., & Lee, H. H. (2021). Virtual impedance control scheme to compensate for voltage harmonics with accurate harmonic power sharing in islanded microgrids. *IEEE Journal of Emerging and Selected Topics in Power Electronics*, *9*(2), 1682-1695. https://doi.org/10.1109/JESTPE.2020.2983447

[13] Wang, Y., Tang, J., Si, J., Xiao, X., Zhou, P., & Zhao, J. (2023). Power quality enhancement in islanded microgrids via closed-loop adaptive virtual impedance control. *Protection and Control of Modern Power Systems*, *8*(1), 10. https://doi.org/10.1186/s41601-023-00284-z

[14] Vijay, A. S., Parth, N., Doolla, S., & Chandorkar, M. C. (2021). An adaptive virtual impedance control for improving power sharing among inverters in islanded AC microgrids. *IEEE Transactions on Smart Grid*, 12(4), 2991-3003. https://doi.org/10.1109/TSG.2021.3062391

[15] Wong, Y. C. C., Lim, C. S., Cruden, A., Rotaru, M. D., & Ray, P. K. (2021). A consensus-based adaptive virtual output impedance control scheme for reactive power sharing in radial microgrids. *IEEE Transactions on Industry Applications*, *57*(1), 784-794. https://doi.org/10.1109/TIA.2020.3031884

[16] Liang, X., Andalib-Bin-Karim, C., Li, W., Mitolo, M., & Shabbir, M. N. S. K. (2021). Adaptive virtual impedance-based reactive power sharing in virtual synchronous generator controlled microgrids. *IEEE Transactions on Industry Applications*, *57*(1), 46-60. https://doi.org/10.1109/TIA.2020.3039223

[17] Xiao, J., Wang, L., Bauer, P., & Qin, Z. (2024). Virtual Impedance Control for Load Sharing and Bus Voltage Quality Improvement in Low Voltage

AC Microgrid. *IEEE Transactions on Smart Grid, 15*(3), 2447-2458. https://doi.org/10.1109/TSG.2023.3325620

[18] Deng, F., Yao, W., Zhang, X., & Mattavelli, P. (2022). A Decentralized current sharing strategy for Islanded resistive microgrids based on iterative virtual impedance regulation. *IEEE Transactions on Industrial Informatics, 18*(6), 3958-3969. https://doi.org/10.1109/TII.2021.3110951

[19] An, R., Liu, Z., & Liu, J. (2020). Successive-approximation-based virtual impedance tuning method for accurate reactive power sharing in islanded microgrids. *IEEE Transactions on Power Electronics, 36*(1), 87-102. https://doi.org/10.1109/TPEL.2020.3001037

[20] Wang, Y., Zhou, X., Tang, J., Xiao, X., Zhang, S., & Si, J. (2024). Adaptive Harmonic Virtual Impedance Control for Improving Voltage Quality of Microgrids. *Journal of Modern Power Systems and Clean Energy, 12*(5), 1548-1558. https://doi.org/10.35833/MPCE.2023.000447

[21] Chen, J., Yue, D., Dou, C., Chen, L., Weng, S., & Li, Y. (2021). A virtual complex impedance based P-V droop method for parallel-connected inverters in low-voltage AC microgrids. *IEEE Transactions on Industrial Informatics, 17*(3), 1763-1773. ttps://doi.org/10.1109/TII.2020.2997054

[22] Nandi, R., Tripathy, M., & Gupta, C. P. (2024). Advanced Adaptive Virtual Impedance Based Dual Mode Inverter Controller for Power and Voltage Coordination in LV AC Microgrid. *IEEE Transactions on Industry Applications, 60*(6), 8495-8508. https://doi.org/10.1109/TIA.2024.3443777

[23] Zhang, X., Yi, H., Wen, Y., Wang, Z., Li, Q., Kang, F., & Zhuo, F. (2024). A Decentralized Nonlinear Harmonic Power Sharing Scheme Considering Harmonic Residual Capacity and Working Conditions of Fundamental Load. *IEEE Transactions on Power Electronics, 39*(11), 14533-14549. https://doi.org/10.1109/TPEL.2024.3432187

[24] Ndeh, S. G., Ngwashi, D. K., Letting, L. K., Iweh, C. D., & Tanyi, E. (2024). Power sharing enhancement through a decentralized droop-based control strategy in an islanded microgrid. *e-Prime-Advances in Electrical Engineering, Electronics and Energy, 7*, 100433. https://doi.org/10.1016/j.prime.2024.100433

[25] Mishra, B., & Pattnaik, M. (2024). A modified droop-based decentralized control strategy for accurate power sharing in a PV-based islanded AC microgrid. *ISA transactions, 153*, 467-481. https://doi.org/10.1016/j.isatra.2024.07.032

[26] AlSadat, M., Ibanez, F. M., Elghanam, I., & Terzija, V. (2024). Using low bandwidth communication through power lines to enhance reactive power sharing for inverters-based microgrids. *International Journal of Electrical Power & Energy Systems, 159*, 110043. https://doi.org/10.1016/j.ijepes.2024.110043

[27] Li, Y., Deng, F., Qi, R., & Lin, H. (2022). Adaptive virtual impedance regulation strategy for reactive and harmonic power sharing among paralleled virtual synchronous generators. *International Journal of Electrical Power & Energy Systems, 140*, 108059. https://doi.org/10.1016/j.ijepes.2022.108059

[28] Goh, H. H., Zhang, X., Zhang, D., Dai, W., Liu, J., Li, G., & Goh, K. C. (2024). Harmonic virtual impedance control in islanded microgrids for harmonic power sharing and harmonic suppression. *CSEE Journal of Power and Energy Systems, (Early Access).*
https://doi.org/10.17775/CSEEJPES.2022.06150

[29] Kim, S., Hyon, S., & An, Y. (2024). Harmonic power sharing control using adaptive virtual harmonic impedance in islanded microgrids. *International Journal of Emerging Electric Power Systems, 25*(2), 135-148. https://doi.org/10.1515/ijeeps-2022-0200

[30] Haghshenas, M. (2024). A Distributed Control Strategy for Load Sharing and Harmonic Compensation in Islanded PV-based Microgrids. *Journal of Solar Energy Research, 9*(2), 1926-1941. https://doi.org/10.22059/JSER.2024.371687.1377.

[31] Hosseinpour, M., Akbari, R., & Shahparasti, M. (2024). A Robust Photovoltaic Power Conditioning System Connected to Weak Grid Through Virtual Impedance Shaping. *Journal of Solar Energy Research, 9*(2), 1870-1886. https://doi.o.rg/10.22059/jser.2024.369348.1364

[32] Ghanizadeh, R., & Gharehpetian, G. B. (2019). Voltage quality and load sharing improvement in islanded microgrids using distributed hierarchical control. *IET Renewable Power Generation, 13*(15), 2888-2898. https://doi.org/10.1049/iet-rpg.2019.0467

[33] Ghanizadeh, R., & Gharehpetian, G. B. (2018). Distributed hierarchical control structure for voltage harmonic compensation and harmonic current sharing in isolated MicroGrids. *Sustainable Energy, Grids and Networks, 16*, 55-69. https://doi.org/10.1016/j.segan.2018.05.005

[34] Savaghebi, M., Jalilian, A., Vasquez, J. C., & Guerrero, J. M. (2012). Secondary control for voltage quality enhancement in microgrids. *IEEE Transactions on Smart Grid, 3*(4), 1893-1902. https://doi.org/10.1109/TSG.2012.2205281

[35] Barklund, E., Pogaku, N., Prodanovic, M., Hernandez-Aramburo, C., & Green, T. C. (2008). Energy management in autonomous microgrid using stability-constrained droop control of inverters. *IEEE Transactions on Power Electronics, 23*(5), 2346-2352.
https://doi.org/10.1109/TPEL.2008.2001910
[36] Nagliero, A., Ricchiuto, D., Mastromauro, R. A., & Liserre, M. (2010). Management of grid-inverter outages and power quality disturbances in distributed power generation systems. *Annual Conference on IEEE Industrial Electronics Society*. 3022-3027
https://doi.org/10.1109/IECON.2010.5674949
[37] IEEE Standard 1459-2010 (2010). IEEE standard definitions for the measurement of electric power quantities under sinusoidal, nonsinusoidal, balanced, or unbalanced conditions. 1-50. https://doi.org/10.1109/IEEESTD.2010.5439063
[38] IEEE Standard 1547-2003 (2003). IEEE Standard for Interconnecting Distributed Resources with Electric Power Systems, 1-28. https://doi.org/10.1109/IEEESTD.2003.94285